Inorganic Chemistry

Article

pubs.acs.org/IC

Homochiral Helical Metal–Organic Frameworks of Group 1 Metals

Daniel L. Reger,* Andrew Leitner, and Mark D. Smith

Department of Chemistry and Biochemistry, University of South Carolina, Columbia, South Carolina 29208, United States

T. Thao Tran and P. Shiv Halasyamani

Department of Chemistry, University of Houston, Houston, Texas 77204, United States

Supporting Information

ABSTRACT: The reactions of (*S*)-2-(1,8-naphthalimido)propanoic acid (HL_{ala}) and (*S*)-2-(1,8-naphthalimido)-3-hydroxypropanoic acid (HL_{ser}), protonated forms of ligands that contain a carboxylate donor group, an enantiopure chiral center, and a 1,8-naphthalimide $\pi\cdots\pi$ stacking supramolecular tecton and in the case of HL_{ser} an alcohol functional group, with the appropriate alkali metal hydroxide followed by a variety of crystallization methods leads to the formation of crystalline $K(L_{ala})(MeOH)$ (**1**), $K(L_{ala})(H_2O)$ (**2**), $Na(L_{ala})(H_2O)$ (**3**), KL_{ser} (**4**), CsL_{ser} (**5**), and CsL_{ala} (**6**). Each of these new complexes has a solid state structure based on six-coordinate metals linked into homochiral helical rod secondary building unit (SBU) central cores. In addition to the bonding of the carboxylate and solvent (in the case of L_{ser} the ligand alcohol) to the metals, both oxygens on the 1,8-naphthalimide act as donor groups. One naphthalimide oxygen bonds to the same helical rod SBU as the carboxylate group of that ligand forming a chelate ring. The other naphthalimide oxygen bonds to adjacent SBUs. In complexes **1**–**3**, this inter-rod link has a square arrangement bonding four other rods forming a three-dimensional enantiopure metal–organic framework (MOF) structure, whereas in **4**–**6** this link has a linear arrangement bonding two other rods forming a two-dimensional, sheet structure. In the latter case, the third dimension is supported exclusively by interdigitated $\pi\cdots\pi$ stacking interactions of the naphthalimide supramolecular tecton, forming enantiopure supramolecular MOF solids. Compounds **1**–**3** lose the coordinated solvent when heating above 100 °C. For **1**, the polycrystalline powder reverts to **1** only by recrystallization from methanol, whereas compounds **2** and **3** undergo gas/solid, single-crystal to single-crystal transformations to form dehydrated compounds **2*** and **3***, and rehydration occurs when crystals of these new complexes are left out in air. The reversible single-crystal to single-crystal transformation of **2** involves the dissociation/coordination of a terminal water ligand, but the case of **3** is remarkable considering that the water that is lost is the only bridging ligand between the metals in the helical rod SBU and a carboxylate oxygen that is a terminal ligand in **3** moves into a bridging position in **3*** to maintain the homochiral helical rods. Both **2*** and **3*** contain five-coordinate metals. There are no coordinated solvents in compounds **4**–**6**, in two cases by designed ligand modification, which allows them to have high thermal stability. Compounds **1**–**3** did not exhibit observable Second Harmonic Generation (SHG) efficiency at an incident wavelength of 1064 nm, but compounds **4**–**6** did exhibit modest SHG efficiency for MOF-like compounds in the range of 30 × α-SiO_2.

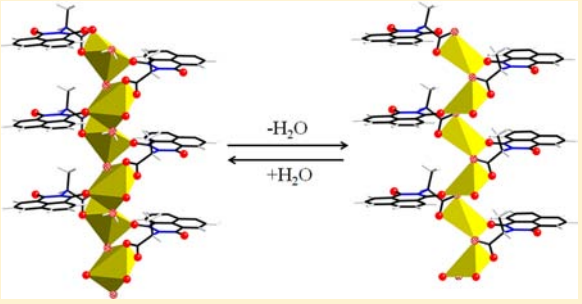

INTRODUCTION

The rational design of metal–organic frameworks (MOFs) with diverse architectures and functionalities is a major area for research because of the wide range of potential applications.[1] Secondary building units (SBUs) are the core geometric building blocks of MOFs that are used to assemble desired structures when coupled with appropriately chosen bridging ligands.[2] In addition to the covalent forces from which these network solids are built, supramolecular tectons (e.g., groups that can hydrogen bond or participate in $\pi\cdots\pi$ stacking interactions) can be built into the organic ligands for added functionality and enhanced stability.[3]

We recently designed a series of ligands with up to four functionalities derived from enantiopure amino acids and a 1,8-naphthalimide group (Scheme 1).[4] The first functionality comes from the carboxylate anion that acts as a donor to the metal cations and helps constitute the SBU.[2] The second is the chiral center from enantiopure amino acids, which imparts chirality on the crystal structure resulting in noncentrosym-

Scheme 1. Enantiopure Tri- and Tetrafunctional Ligands

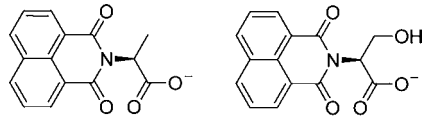

L_{ala}^- L_{ser}^-

Received: May 28, 2013
Published: August 14, 2013

   dx.doi.org/10.1021/ic401327h | *Inorg. Chem.* 2013, 52, 10041–10051

metric space groups.[4,5] The third key feature of the amino acid component is the "side chain" that can contain functional groups such as an alcohol or amide. The fourth, and probably most unique feature of the ligands is the 1,8-naphthalimide group that not only blocks the amine end of the acid from coordination,[6] but has been shown to organize the supramolecular structure through directionally versatile and strong $\pi\cdots\pi$ stacking interactions.[4,7,8]

The majority of our previous research on metal complexes of these ligands has dealt with the square paddlewheel SBU adopted by late transition metals.[7] These and related studies have demonstrated that ligands containing the 1,8-naphthalimide group have complex structures frequently organized in at least one dimension by supramolecular interactions, structural types that we have denoted as supramolecular metal−organic frameworks (SMOFs).[7b] These SMOFs have shown very interesting properties, most notably a variety of single-crystal to single-crystal transformations; in one system gas/solid guest exchange takes place in densely packed solids,[4a] in another the gas/solid exchange is enantioselective with a racemic substrate,[7a] and in a third temperature induced phase changes are observed.[4c] To investigate additional interesting trends and physical properties imparted by these ligands, we chose to look at complexes with group 1 metals. Although not as extensively studied in this field as transition metals, s-block metals are cheap, nontoxic, and essential in many biological processes,[9] and their complexes have shown a wealth of interesting properties, ranging from catalysts[10] to ferroelectrics.[11] By using enantiopure ligands the new complexes can also have interesting nonlinear optical applications. Herein we report the syntheses and structures of eight alkali metal complexes of three different group 1 metals with the two ligands pictured in Scheme 1 along with their thermal, fluorescent and nonlinear optical properties. In contrast to other studies with these metals,[12] two very similar structural types have emerged from this study, both of which are based on homochiral rod SBUs, despite changes in metals, ligands, and solvent systems. Two of these compounds are able to undergo reversible single-crystal to single-crystal transformations even though the solids lack channels. Some of these results have been communicated previously.[13]

EXPERIMENTAL SECTION

General Considerations. All reactants were used as purchased from Aldrich and Strem. The syntheses of the ligands HL_{ala} and HL_{ser} have been reported elsewhere.[4c,8,13] Elemental analyses were performed by Robertson Microlit Laboratories (Ledgewood, NJ). Thermal gravimetric analysis was performed using a Thermal Analysis (TA) SDTQ600 simultaneous DTA/TGA system. The samples were heated in dry air to 800 °C with a heating rate of 10 °C/min. Some samples (compounds **3** and **6**) froth when heated too high, so the experiment was terminated after the decomposition temperature was recorded. The fluorescence measurements were done on a Perkin-Elmer Lambda 35 UV−vis spectrometer.

$K(L_{ala})(MeOH)$ (1). HL_{ala} (2.0 g, 7.4 mmol) was added to a solution of potassium hydroxide (0.42 g, 7.4 mmol) in water and stirred for an hour until homogeneous. The solvent was removed, and the precipitate dried in vacuo to produce a light brown powder (1.96 g). A 9 mL thick walled glass tube with a Teflon screw top was charged with a sample of this solid (0.10 g) and methanol (4 mL) and heated at 120 °C overnight or until the solution became homogeneous. The heat was removed, and the system was allowed to slowly cool at a rate of about 1 °C/min. The reaction vessel was placed in a quiet area. Over the course of 3 days large crystals grew from the solution and were collected from the tube and washed with diethyl ether to provide 0.063 g of single crystals. Anal. Calcd. (Found) for $C_{16}H_{12}KNO_5$: C 56.62 (56.42); H 4.16 (4.00); N 4.13 (3.97).

$K(L_{ala})(H_2O)$ (2). The light brown powder of KL_{ala} (0.086 g, 0.28 mmol) was dissolved in water (1 mL), and acetone vapor was allowed to diffuse into the solution to yield X-ray quality single crystals (0.064 g) after 3 weeks. Anal. Calcd. (Found) for $C_{15}H_{12}KNO_5$: C 55.37 (55.21); H 3.72 (3.58); N 4.31 (4.28).

$Na(L_{ala})(H_2O)$ (3). HL_{ala} (1.30 g, 4.83 mmol) was added to a solution of sodium hydroxide (0.20 g, 5.0 mmol) in methanol (30 mL) and stirred until homogeneous. The solution was filtered through a short Celite plug. The solvent was removed, and the resulting precipitate dried in vacuo to produce a pale orange powder (1.30 g). A 9 mL thick walled glass tube with a Teflon screw top was charged with the solid (0.05 g), a 40:1 mixture of 1-butanol and water (4 mL) was added and heated at 120 °C overnight or until the solution became homogeneous. The heat was removed, and the system was allowed to slowly cool at a rate of about 1 °C/min. The reaction vessel was placed in a quiet area. Over the course of 2 days large crystals grew from the solution and were collected from the tube and washed with diethyl ether to provide 0.032 g of single crystals. Anal. Calcd. (Found) for $C_{15}H_{14}NNaO_5$: C 58.26 (58.08); H 3.91 (3.93); N 4.53 (4.44).

$K(L_{ser})$ (4). HL_{ser} (1.00 g, 3.5 mmol) was added to a solution of potassium hydroxide (0.20 g, 3.5 mmol) in water and stirred for an hour or until homogeneous. The solvent was removed, and the precipitate dried in vacuo to produce a light brown powder (0.89 g). A 9 mL thick walled glass tube with a Teflon screw top was charged with the solid (0.05 g) and methanol (2.0 mL) and heated at 120 °C. Over the course of heating for 3 days, brown crystals grew on the walls of the tube above the solvent line. After no starting material remained at the bottom of the tube, the heat was removed, and the system was allowed to slowly cool at a rate of about 1 °C/min. Small dark brown crystals were collected from the walls of the tube and washed with diethyl ether to provide 0.032 g of single crystals. Anal. Calcd. (Found) for $C_{15}H_{10}KNO_5$: C 55.72 (55.60); H 3.12 (3.22); N 4.33 (4.21).

$Cs(L_{ser})$ (5). This compound was prepared by the same procedure as for KL_{ser}, but with $CsOH{\cdot}xH_2O$ (0.50 g) and HL_{ser} (0.72 g, 2.5 mmol) to provide a pale brown powder (1.02 g). Small dark brown crystals were collected from the walls of the tube and washed with diethyl ether to provide 0.031 g of single crystals. Anal. Calcd. (Found) for $C_{15}H_{10}CsNO_4$: C 44.91 (44.38); H 2.51 (2.33); N 3.49 (3.31).

$Cs(L_{ala})$ (6). This compound was prepared by the same procedure as for KL_{ser}, but with $CsOH{\cdot}xH_2O$ (0.50 g) and HL_{ala} (0.76 g, 2.5 mmol) to provide an orange powder (1.06 g). Small dark brown crystals were collected from the walls of the tube and washed with diethyl ether to provide 0.037 g of single crystals. Anal. Calcd. (Found) for $C_{15}H_{10}CsNO_5$: C 43.19 (43.10); H 2.42 (2.31); N 3.36 (3.36).

Second Harmonic Generation (SHG) Studies. Powder SHG measurements were performed on a modified Kurtz-nonlinear optical (NLO) system using a pulsed Nd:YAG laser with a wavelength of 1064 nm.[14] A detailed description of the equipment and methodology has been published.[15] As the powder SHG efficiency has been shown to strongly depend on particle size,[14] **4**, **5**, and **6** were ground and sieved into distinct particle size ranges (<20, 20−45, 45−63, 63−75, 75−90, >90 μm). Relevant comparisons with known SHG materials were made by grinding and sieving crystalline α-SiO_2 and $LiNbO_3$ into the same particle size ranges. No index matching fluid was used in any of the experiments.

Powder X-ray Diffraction. To test for phase purity of the crystalline products, samples for compounds **1**−**5** were collected from the walls of the solvothermal tubes, washed with diethyl ether and ground in air. For compound **6** the single crystals were transported into a drybox and ground in a nitrogen atmosphere. A zero-background slide was loaded with the sample, covered with a Kapton film and sealed with high vacuum grease. All measurements were performed on a Rigaku Ultima 4 instrument using Cu Kα radiation at a scan rate of 1°/min between 5 and 30° 2θ with a step size of 0.02° 2θ. Powder patterns were analyzed using Microsoft Excel. These powder patterns are shown in the Supporting Information, Figures S8−S13, and demonstrate phase purity for **1**−**5**. A similar analysis with **6** initially indicated some lack of phase purity, but two additional short

Table 1

	1	2	2*	3	3*	4	5	6
formula	$C_{16}H_{14}KNO_5$	$C_{15}H_{12}KNO_5$	$C_{15}H_{10.58}KNO_{4.29}$	$C_{15}H_{12}NaNO_5$	$C_{15}H_{10}NaNO_4$	$C_{15}H_{10}KNO_5$	$C_{15}H_{10}CsNO_5$	$C_{15}H_{10}CsNO_4$
Fw, g mol^{-1}	339.38	325.36	312.58	309.25	291.23	323.34	417.15	401.15
cryst. syst.	orthorhombic	orthorhombic	orthorhombic	orthorhombic	orthorhombic	monoclinic	monoclinic	monoclinic
space group	$P2_12_12_1$	$P2_12_12_1$	$P2_12_12_1$	$P2_12_12_1$	$P2_12_12_1$	$P2_1$	$P2_1$	$P2_1$
T, K	100(2) K	100(2) K	100(2) K	100(2) K	100(2) K	100(2) K	100(2) K	100(2) K
a, Å	6.8979(5)	6.9520(7)	6.874(2)	6.9818(7)	6.9329(13)	8.7050(5)	9.2965(12)	9.0674(6)
b, Å	14.3515(10)	13.2676(13)	12.842(4)	11.8361(13)	12.061(2)	6.6081(4)	6.6108(9)	6.5650(5)
c, Å	14.5164(10)	14.9719(15)	15.052(4)	15.5125(17)	14.777(3)	11.1731(7)	11.2603(15)	11.2571(8)
a, deg	90	90	90	90	90	90	90	90
P, deg	90	90	90	90	90	99.1048(10)	99.668(2)	95.2910(10)
Y, deg	90	90	90	90	90	90	90	90
V, A^3	1437.05(18)	1381.0(2)	1328.8(7)	1281.9(2)	1235.5(4)	634.62(7)	682.20(16)	667.25(8)
Z	4	4	4	4	4	2	2	2
R1 ($I > 2\sigma(I)$)	0.0277	0.0296	0.0439	0.0322	0.0522	0.0311	0.0233	0.0233
wR2 ($I > 2\sigma(I)$)	0.0721	0.0748	0.1085	0.0830	0.1306	0.0819	0.0552	0.0546
Flack parameter	0.01(4)	−0.03(4)	0.05(7)	n/a	n/a	0.03(3)	0.01(2)	0.037(16)

scans (10−15° 2θ at a scan rate of 2°/min) were performed on compound **6**, before and after the long scan, and they show that compound **6** likely undergoes a change when ground and the measurement carried out (Supporting Information, Figure S14).

Recycling Experiments. The repeated single-crystal to single-crystal transformation of compound **3** to **3*** was performed on two selected single crystals. These crystals were collected from the walls of the solvothermal tubes and washed with diethyl ether. After checking the unit cell, they were heated under vacuum to 150 °C for 1 h in a Schlenk flask. The flask was refilled with nitrogen, and the crystal quickly mounted in a nitrogen cold stream on the diffractometer; the unit cell parameters were collected, and the diffraction peaks monitored for broadening to determine if compound **3*** had formed and retained single crystallinity. These same two single crystals were then returned to a glass vial which was kept in a humid environment for two days, and unit cell parameters collected to determine if compound **3** had reformed. This procedure was repeated; at the end the single crystals started to show broadening in the diffraction pattern indicating some degradation had taken place.

Crystallographic Studies. For all complexes, X-ray diffraction intensity data were measured at 100(2) K using a Bruker SMART APEX diffractometer (Mo Kα radiation, λ = 0.71073 Å).[16] The raw area detector data frames were reduced with the SAINT+ program.[16] Direct methods structure solution, difference Fourier calculations, and full-matrix least-squares refinement against F^2 were performed with SHELXS/L, implemented in OLEX2.[17,18] Non-hydrogen atoms were refined with anisotropic displacement parameters. Hydrogen atoms bonded to carbon were placed in geometrically idealized positions and included as riding atoms. For compounds **1**, **2**, **2***, **4**, **5**, and **6**, crystal enantiopurity and the "S" configuration of the chiral carbon (C13 in all structures) were established by the absolute structure (Flack) parameters of zero (within experimental error) derived from the X-ray data sets. For **3** and **3***, containing no atoms heavier than sodium in the crystal, the absolute structures were inferred from synthetic information; that is, enantiopure starting material which does not racemize. Details of data collection are given in Table 1, and the solution and refinement of structures is detailed in the Supporting Information.

RESULTS

Syntheses. The reaction of HL_{ala} and HL_{ser} with the appropriate alkali metal hydroxide (NaOH, KOH, CsOH) in water or methanol produced NaL_{ala}, KL_{ala}, CsL_{ala}, KL_{ser}, and CsL_{ser}. Crystals of K(L_{ala})(MeOH) (**1**) and Na(L_{ala})(H_2O) (**3**) were obtained by heating the appropriate salt in an alcohol solution to 120 °C followed by cooling. Crystals of KL_{ser} (**4**), CsL_{ser} (**5**), and CsL_{ala} (**6**) were obtained by solvothermal treatment in alcohol solution at 120 °C and grew on the walls of the reaction vessel above the solvent line. Dissolving KL_{ala} in water followed by vapor diffusion of acetone into the solution afforded crystals of K(L_{ala})(H_2O) (**2**).

Structural Analyses. In K(L_{ala})(MeOH) (**1**), the potassium cation is 6-coordinate with two of the sites occupied by μ^2-κ^2 carboxylate oxygens, two by bridging methanols, and two by carbonyls from the naphthalimide rings (Figure 1). One of

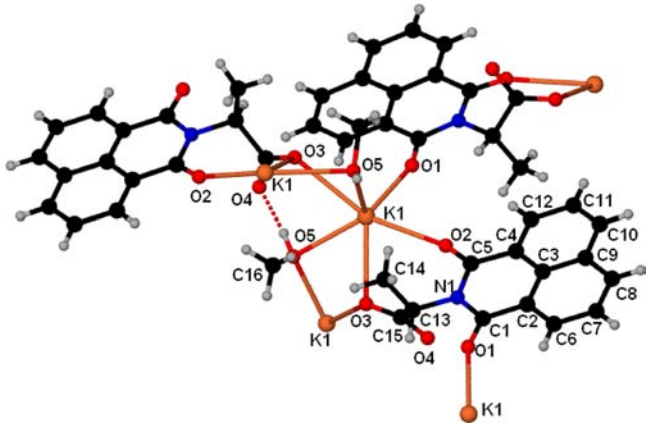

Figure 1. K^+ coordination environment of K(L_{ala})(MeOH) (**1**); black, C; red, O; blue, N; white, H; orange, K.

the naphthalimide carbonyls is coordinated to a potassium cation in the same chain as the bridging carboxylate oxygen of that ligand forming a seven-member chelate ring. The noncoordinated oxygen atom from the carboxylate participates in hydrogen bonding to the methanol bridging to the next potassium cation. The irregular potassium polyhedra are edge-shared through the bridging oxygen atoms originating from the methanol and carboxylate, extending in one dimension to generate helical rods. The helical rods are enantiopure, all *P*-handed helicies as defined by the K1−O3−K1−O3 chain (Figure 2) with a pitch of 6.90 Å. The second naphthalimide carbonyl of each ligand acts to bridge adjacent helices. These

dx.doi.org/10.1021/ic401327h | *Inorg. Chem.* 2013, 52, 10041−10051

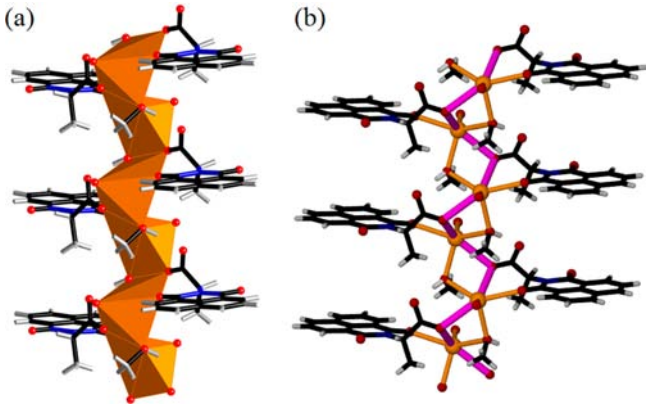

Figure 2. (a) Rod-like structure of **1** formed by edge shared K^+ polyhedra and (b) the *P*-handed helix highlighted in purple follows the K1−O3−K1−O3 chain.

bridging naphthalimide carbonyls form four points of extension from each helical rod generating "squares" which are occupied by the naphthalimide rings (Figure 3), generating a three-dimensional uninodal 4*c* net structure.

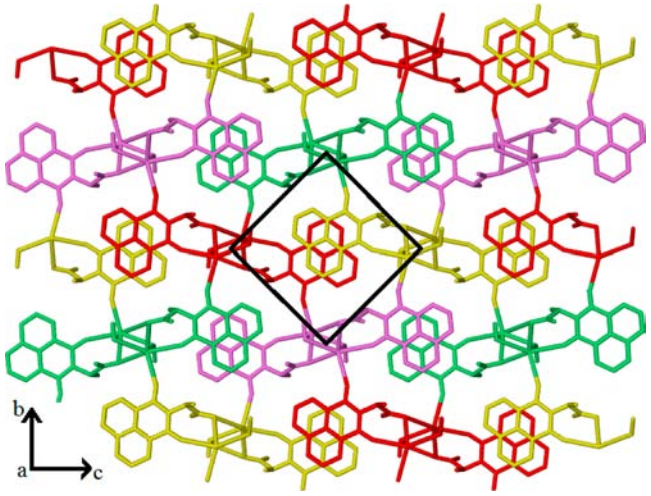

Figure 3. View down the crystallographic *a* axis of **1** illustrating the four points of connectivity between rods, where each rod is a different color and the vertices of the square lie in the center of each helical rod.

The naphthalimide rings form extended $\pi\cdots\pi$ stacking networks that reinforce the structure. Four parameters were chosen to define the strength of the naphthalimide $\pi\cdots\pi$ stacking interaction: the dipole angle between the two rings, the angle between ring planes, the average perpendicular distance, and the slippage parameter (χ) that is defined as the third side of the right triangle formed with the average perpendicular distance between the two rings and the line between the two central carbon atoms of the rings. The values for these metrics, along with the angles formed by the dipole vectors of the rings, are listed in Table 2.

The structure of $K(\mathbf{L}_{ala})(H_2O)$ (**2**) is very similar to **1** with the presence of homochiral helical rods of potassium cations and the uninodal 4*c* net, yet there are important differences in the coordination environment and helical connectivity. The potassium is 6-coordinate with three of the sites occupied by the μ^2-κ^1:κ^2 carboxylate oxygens, one of the sites filled by a terminal water molecule, and the remaining two sites filled by two carbonyls from the naphthalimide rings (Figure 4). The

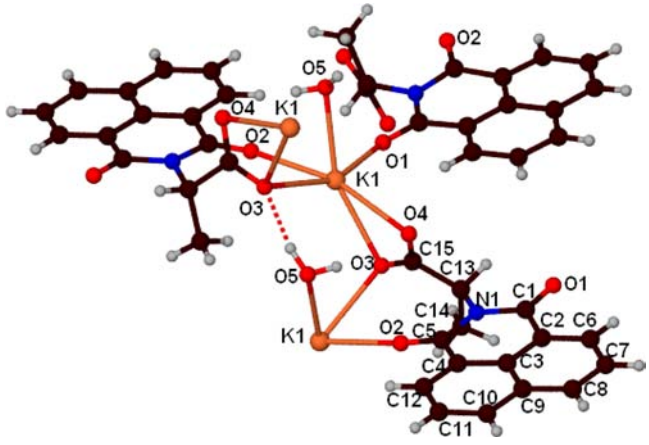

Figure 4. K^+ coordination environment of $K(\mathbf{L}_{ala})(H_2O)$ (**2**); black, C; red, O; blue, N; white, H; orange, K.

terminal water molecule in **2** is hydrogen bonded to the carboxylate O3 involved with bridging the next two potassium cations of the helix. The distorted octahedral potassium polyhedra are corner-shared through the bridging carboxylate and extend in one dimension to generate helical rod SBUs. The *P*-handed helix defined by the K1−O3−K1−O3 chain is shown in Figure 5 and has a pitch of 6.95 Å. As with **1**, one of the

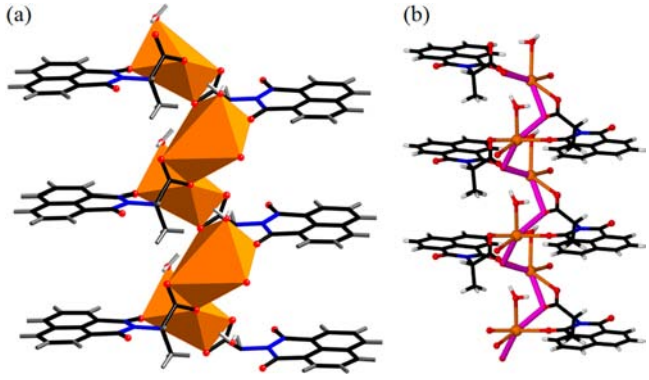

Figure 5. (a) Rod-like structure of **2** formed by corner shared K^+ polyhedra and (b) the *P*-handed helix highlighted in purple follows the K1−O3−K1−O3 chain.

Table 2. $\pi\cdots\pi$ Stacking Metrics for Compounds 1−3

	compound	cen-cen (Å)	dipole ∠ (deg)	plane ∠ (deg)	avg dist (Å)	χ (Å)
1	$K(\mathbf{L}_{ala})(MeOH)$	3.70	180	4.8	3.45	1.34
2	$K(\mathbf{L}_{ala})(H_2O)$	3.67	180	2.9	3.48	1.16
2*	$K(\mathbf{L}_{ala})(H_2O)_{0.29}$	3.63	180	3.6	3.45	1.16
3	$Na(\mathbf{L}_{ala})(H_2O)$	3.77	180	5.9	3.49	1.43
3*	$Na(\mathbf{L}_{ala})$	3.66	180	3.8	3.46	1.18

dx.doi.org/10.1021/ic401327h | *Inorg. Chem.* 2013, 52, 10041−10051

naphthalimide carbonyls is coordinated to a potassium cation in the same chain as the bridging carboxylate oxygen of that ligand forming a seven-member chelate ring, while the other acts to bridge an adjacent helix. The bridging mode of the naphthalimide carbonyls again creates four points of extension per rod, and the extended interdigitated $\pi\cdots\pi$ stackings are similar to compound **1** (Supporting Information, Figure S1). The metrics for the $\pi\cdots\pi$ stacking are listed in Table 2.

Compound **2** undergoes a reversible single-crystal to single-crystal transformation at high temperatures by the loss of the coordinated water to form compound **2*** (vide infra). The structure of the dehydrated complex is almost identical to the hydrated form with the exception of the coordination number of potassium changing from 6 to 5 (Figure 6) and a slight decrease in the unit cell volume (~3%).

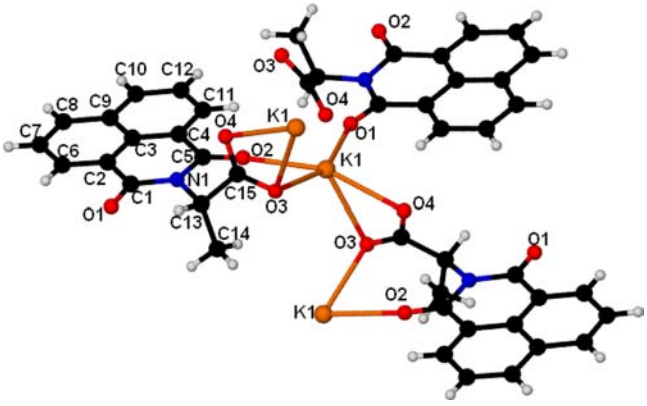

Figure 6. K^+ coordination environment of $K(\mathbf{L}_{ala})$ (**2***); black, C; red, O; blue, N; white, H; orange, K.

$Na(\mathbf{L}_{ala})(H_2O)$ (**3**) again has the same basic structure featuring homochiral helical rods of sodium and a uninodal 4*c* net, but with distinct differences in coordination and helical environment from either **1** or **2**. Sodium is 6-coordinate with two of the sites occupied by a κ^2 carboxylate, two of the sites filled by bridging water molecules, and the remaining two sites filled by two carbonyls from the naphthalimide rings (Figure 7). Compound **3** is the only example where the carboxylate does not act as a bridge and the intrachain chelate ring formed by

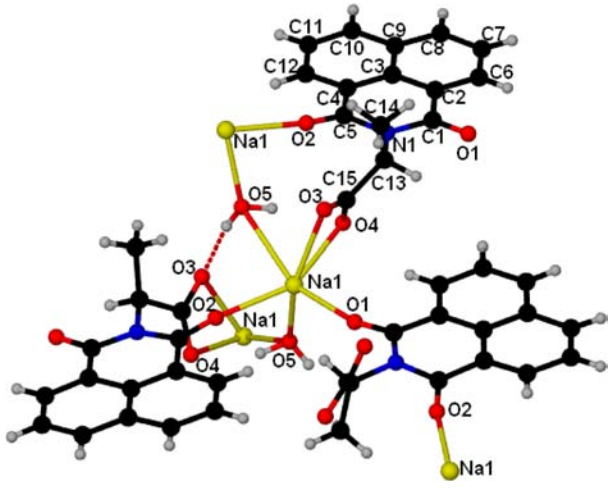

Figure 7. Na^+ coordination environment of $Na(\mathbf{L}_{ala})(H_2O)$ (**3**); black, C; red, O; blue, N; white, H; yellow, Na.

one of the naphthalimide carbonyls involves a sodium located in the next segment of the helix forming nine-member rings. In a similar manner to the methanol in **1**, the bridging water molecule in **3** is hydrogen bonded to the carboxylate O3, but in this case O3 is coordinated to sodium. The distorted octahedral sodium polyhedra are corner shared through the bridging water and extend in one dimension to generate helical rod SBUs (Figure 8). The *P*-handed helix is defined by the Na1−O5−

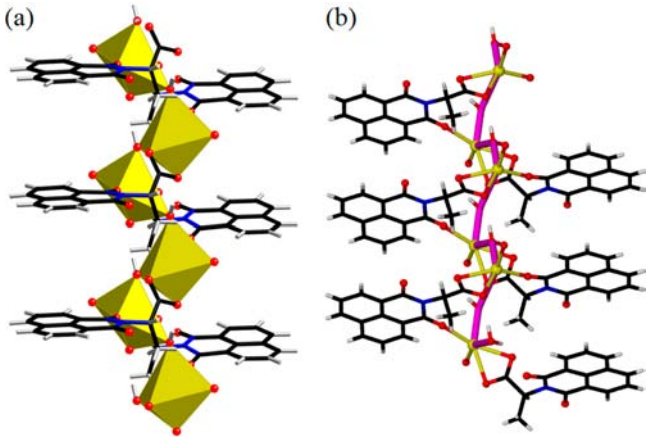

Figure 8. (a) Rod-like structure of **3** formed by corner shared Na^+ polyhedra and (b) the *P*-handed helix highlighted in purple follows the Na1−O5−Na1−O5 chain.

Na1−O5 chain and has a pitch of 6.98 Å. Again, the second naphthalimide carbonyls of each ligand bridge to adjacent helices forming four points of extension per rod, and extended interdigitated $\pi\cdots\pi$ stacking as in compounds **1** and **2** (Supporting Information, Figure S2) is also present. The metrics for the $\pi\cdots\pi$ stacking are listed in Table 2.

Compound **3** undergoes a reversible single-crystal to single-crystal transformation upon heating with loss of water to form compound **3*** (vide infra) which was characterized by single crystal X-ray diffraction. Sodium is 5-coordinate in compound **3*** with 3 of the sites occupied by the μ^2-κ^1:κ^2 carboxylate oxygens in a similar fashion to compound **2**, and the remaining two sites are occupied by the carbonyls of the naphthalimide rings (Figure 9). In comparison to the structure of **3**, the bridging water is lost and one of the oxygens (O3) of the nonbridging, κ^2-carboxylate in **3** moves into a bridging position in the structure of **3***. This change causes the nine-member rings formed by the carboxylate ligand and naphthalimide carbonyls in **3** to become a seven-member ring, similar to that observed in complexes **1** and **2**. Sodium polyhedra are corner-shared through the carboxylate O3 and extend into helical rods (Figure 10). The second naphthalimide carbonyl of each ligand is involved with bridging adjacent rods. The overall 3D structures are the same as those of the previous four compounds where each of the homochiral helical rods of corner-shared sodium atoms are connected to four adjacent rods generating a uninodal 4*c* net (Supporting Information, Figure S3). The metrics for the $\pi\cdots\pi$ stacking are listed in Table 2.

In the structure of $K(\mathbf{L}_{ser})$ (**4**), potassium is 6-coordinate with two of the sites occupied by μ^2-κ^2 carboxylate oxygens, two are filled by the bridging alcohol functional groups located in the side-chains, and the last two are occupied by carbonyls of naphthalimide rings (Figure 11). The *designed ligand*

dx.doi.org/10.1021/ic401327h | *Inorg. Chem.* 2013, 52, 10041−10051

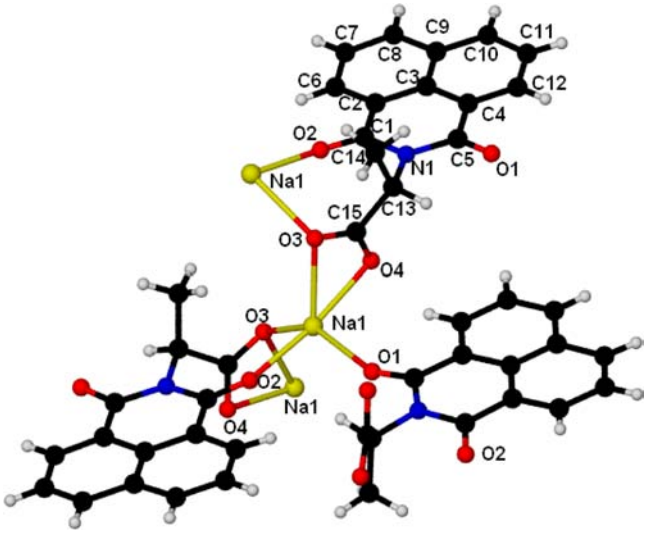

Figure 9. Na^+ coordination environment of $Na(L_{ala})$ (**3***); black, C; red, O; blue, N; white, H; yellow, Na.

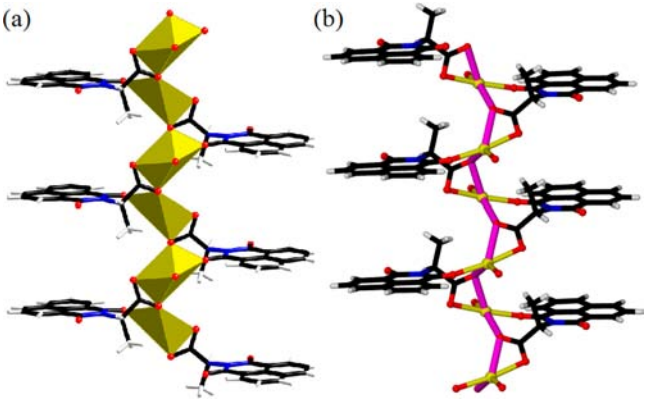

Figure 10. (a) Rod-like structure of **3*** formed by corner shared Na^+ polyhedra and (b) the *P*-handed helix highlighted in purple follows the Na1−O3−Na1−O3 chain.

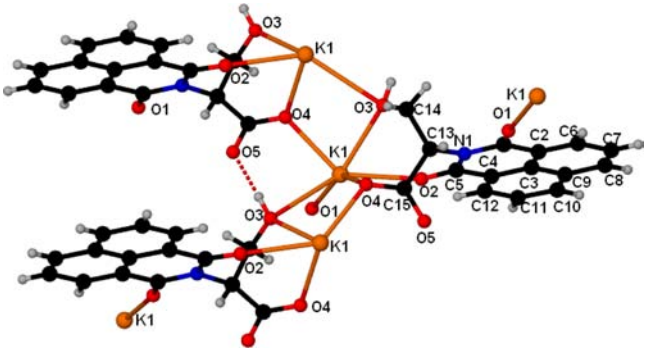

Figure 11. K^+ coordination environment of KL_{ser} (**4**); black, C; red, O; blue, N; white, H; orange, K.

modification in L_{ser}^- when compared to L_{ala}^- introduces the alcohol in the side-chain that replaces the solvent molecules in the structures of **1**−**3**. One of the naphthalimide carbonyls in each ligand is bonded to the same potassium cation as the carboxylate and alcohol that each bridge a different potassium cation in the same chain, forming a [3.2.2] bicyclic system. The distorted trigonal prismatic potassium polyhedra are edge-shared through the bridging alcohol and carboxylate oxygens and extend in one dimension to generate helical rods (Figure 12). The *P*-handed helical rods are defined by the K1−O4−

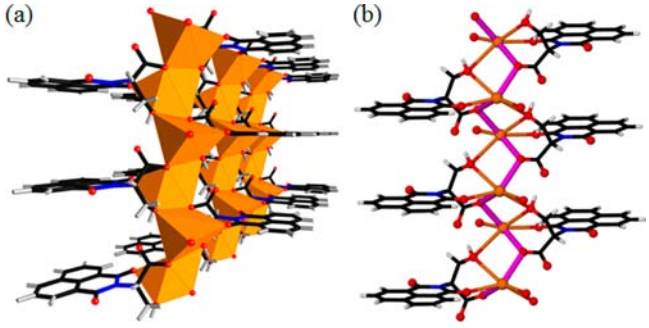

Figure 12. (a) Sheet of rods from **4** formed by edge shared K^+ polyhedra bridged together by the carbonyls of the naphthalimide and (b) the *P*-handed helix of each rod highlighted in purple follows the K1−O4−K1−O4 chain.

K1−O4 chain and have a pitch of 6.61 Å. The other naphthalimide carbonyls in each ligand bridge to potassium cations in adjacent helices. In contrast to **1**−**3**, these connections extend in only two directions, connecting the rods into sheets. All of the naphthalimide rings are pointed away from the helices, fixed in position by the tridentate coordination mode of the ligand, and line up in parallel ribbons. The naphthalimide rings are interdigitated through $\pi\cdots\pi$ stacking connecting the sheets into a three-dimensional supramolecular metal−organic framework (SMOF) in a "zipper-like" fashion as shown in Figure 13. By introducing a

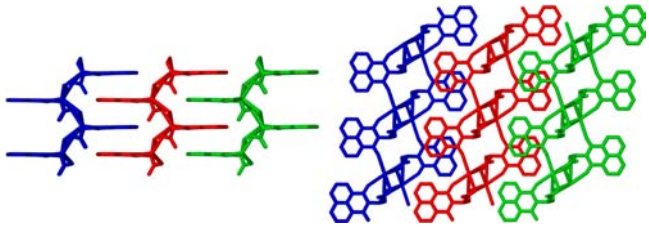

Figure 13. Views down the crystallographic *a* (left) and *c* (right) axis of **4** illustrating the zipperlike $\pi\cdots\pi$ stacking extending the structure in three dimensions and slippage of the naphthalimide rings. Each sheet is distinguished with a different color. Hydrogen atoms are omitted for clarity.

donor group into the ligand side chain, we successfully exclude coordinated solvents, but the ligand is now locked into a different orientation and a new structure type is formed. The metrics for the $\pi\cdots\pi$ stacking are listed in Table 3.

$Cs(L_{ser})$ (**5**) has a very similar structure to **4**. Cesium has an unusually low coordination number of 6 with two of the sites occupied by μ^2-κ^2 carboxylate oxygens, two are filled by the bridging alcohol side-chains, and the last two are filled by carbonyls of the naphthalimide rings (Figure 14). The distorted trigonal prismatic cesium polyhedra are edge-shared through the bridging alcohol and carboxylate oxygens and extend in one dimension to generate helical rods as shown in Figure 15. The *P*-handed helical rods are defined by the Cs1−O4−Cs1−O4 chain and have a pitch of 6.61 Å. The rods are bridged together by carbonyls of the naphthalimide groups extending in two directions to form sheets. These sheets are zippered together

dx.doi.org/10.1021/ic401327h | *Inorg. Chem.* 2013, 52, 10041−10051

Table 3. $\pi\cdots\pi$ Stacking Metrics for Compounds 4−6

	compound	cen-cen(A)	dipole ∠ (deg)	plane ∠ (deg)	avg dist (Å)	χ (Å)
4	K($\mathbf{L}_{ser}$)	4.18	180	1.6	3.30	2.56
5	Cs($\mathbf{L}_{ser}$)	4.32	180	1.5	3.31	2.78
6	Cs($\mathbf{L}_{ala}$)	4.53	180	10.3	3.27	3.11

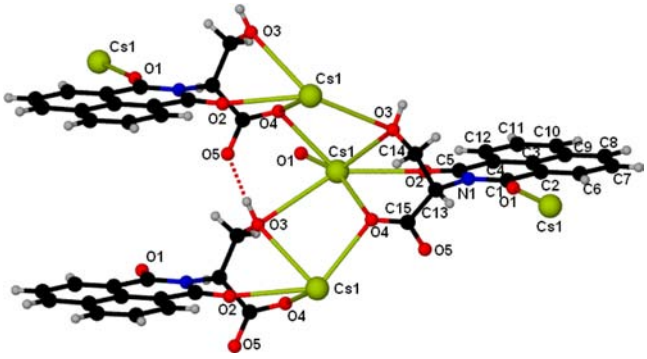

Figure 14. Cs^+ coordination environment of Cs$\mathbf{L}_{ser}$ (5); black, C; red, O; blue, N; white, H; yellow, Cs.

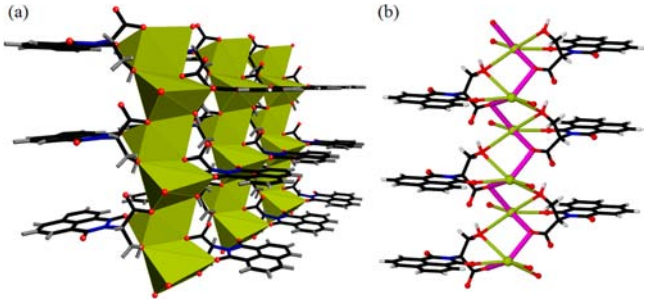

Figure 15. (a) Sheet of rods from 5 formed by edge shared Cs^+ polyhedra bridged together by the carbonyls of the naphthalimide and (b) the *P*-handed helix of each rod highlighted in purple follows the Cs1−O4−Cs1−O4 chain.

through $\pi\cdots\pi$ stacking in a similar fashion to 4 (Supporting Information, Figure S4). The metrics for the $\pi\cdots\pi$ stacking are listed in Table 3.

The coordination environment for the alkali cation in Cs($\mathbf{L}_{ala}$) (6) is significantly different from 1−5, yet the overall 3D structure is very similar to 4 and 5. Compound 6 is the only complex with $\mathbf{L}_{ala}^-$ to exclude the solvent molecule in the structure. Cesium is 6-coordinate with four of the sites occupied by μ^2-κ^2:κ^2 carboxylate oxygens and the remaining two filled by carbonyls of the naphthalimide rings (Figure 16). The unique μ^2-κ^2:κ^2-bonding of the carboxylate group allow the cesium cations to be six-coordinate without the presence of the solvent molecule in 1−3. The cesium cation is in an extremely distorted, low-coordination environment with all of the oxygen donor atoms on one side leaving an open face on the metal. The distance between cesium and the hydrogen atoms of the methyl group of the ligand is short enough (3.17 Å) to denote a Cs···H interaction (Figure 16b). There is also an interaction between cesium and an aromatic hydrogen atom from an adjacent sheet with a distance of 3.32 Å. The irregular cesium polyhedra are edge-shared through both carboxylate oxygens, O3 and O4, and extend in one dimension to generate the helical rod SBU. The *P*-handed helical rods are defined by the Cs1−O4−Cs1−O4 chain and have a pitch of 6.56 Å. One of the carbonyls of the naphthalimide is bonded to the same

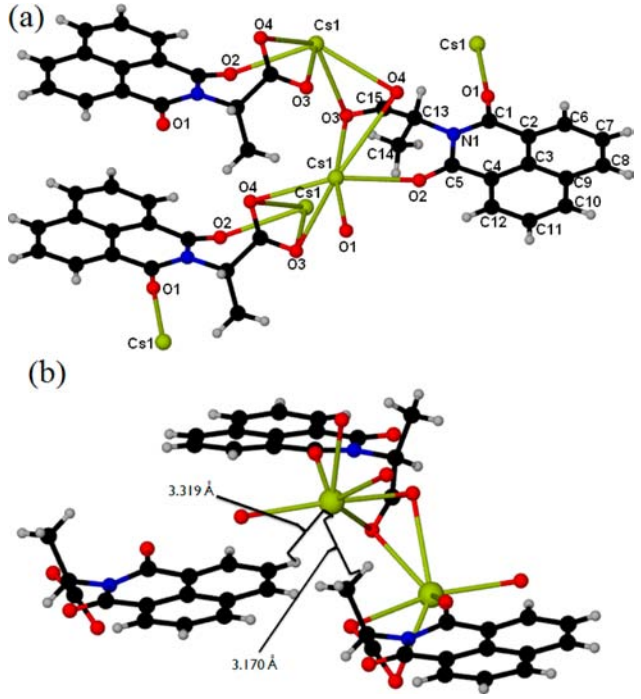

Figure 16. (a) Cs^+ coordination environment of Cs$\mathbf{L}_{ala}$ (6) and (b) possible Cs···H interactions; black, C; red, O; blue, N; white, H; yellow, Cs.

cesium cation as the carboxylate making the ligand tridentate to one metal as in 4 and 5 and generating a [4.1.1] bicyclic system. As in these two structures, the other naphthalimide carbonyls bridge to potassium cations in adjacent helices, again extending in only two directions forming sheets of helical rods (Figure 17). There is $\pi\cdots\pi$ stacking between the naphthalimide rings linking sheets together into a SMOF in the same motif as 4 and 5 (Supporting Information, Figure S5). The metrics for the $\pi\cdots\pi$ stacking are listed in Table 3.

Thermal Analysis. Thermal gravimetric analysis was performed on a TA Instruments SDT 2960 under a steady stream of dry air. Thermal analysis of compounds 1 and 4 are

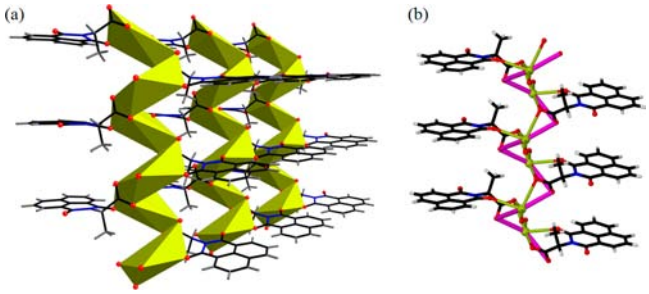

Figure 17. (a) Sheet of rods from 6 formed by rods of edge shared Cs^+ polyhedra bridged together by the carbonyls of the naphthalimide and (b) the *P*-handed helix of each rod highlighted in purple follows the Cs1−O4−Cs1−O4 chain.

dx.doi.org/10.1021/ic401327h | *Inorg. Chem.* 2013, 52, 10041−10051

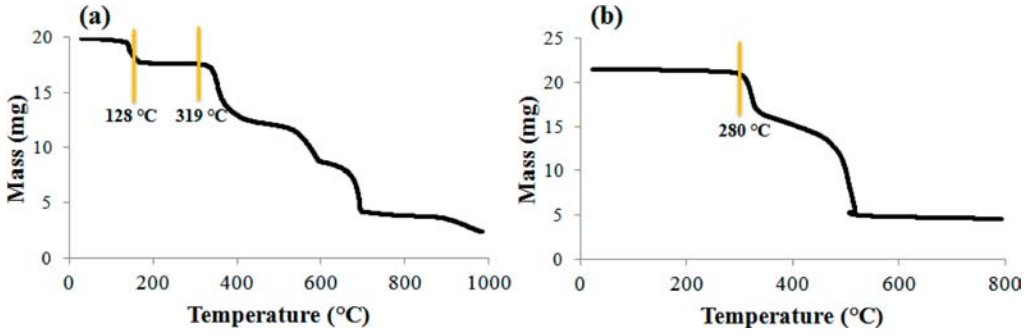

Figure 18. Thermal gravimetric analysis for compounds **1** and **4**.

representative of their structure types and are shown in Figure 18. Compound **1** showed a weight loss at 128 °C that corresponds with a loss of the coordinated methanol ligand (9.81%, calcd. 9.44%). In addition, a physical change from dark brown single crystals to a white polycrystalline powder (**1p**) was observed at this temperature. The powder X-ray diffraction (PXRD) of this powder reveals that although the solid is polycrystalline, the structure has changed. Single crystals of the **1** can be reformed by recrystallization of this solid from methanol, as indicated in the Synthesis section. The polycrystalline powder remains stable until decomposition sets in starting at 319 °C.

Thermogravimetric analysis (TGA) of compound **2** showed a weight loss between 80 and 120 °C corresponding to the loss of the coordinated water ligand (6.00%, calcd. 5.54%), resulting in the formation of a new compound, **2***. Single crystal X-ray analysis of **2***, formed by heating crystals of **2** at 140 °C for 3 h, showed a partially hydrated compound with a 29% occupancy of coordinated water where the remaining potassium cations are five coordinate. Because the TGA shows a quantitative loss of water, we assume that partial rehydration occurred in the short time transferring the single crystals from the nitrogen atmosphere into the paraffin liquid for the X-ray analysis. PXRD analysis shows **2*** is different from **1p**. Upon further heating, compound **2*** experiences a higher decomposition point (347 °C) than **1p** even though they share the same chemical formula. After exposure of the single crystal used for the structure of **2*** to air for two days compound **2** is reformed by reuptake of water, as confirmed by *single-crystal XRD*.

Upon heating, compound **3** experienced a weight loss between 89 and 177 °C indicative of a loss of the *coordinated* water ligand from the structure (6.40%, calcd. 5.83%). A second TGA experiment was performed where the heat ramp was stopped at 160 °C and after sitting in air at room temperature for three days the compound regained the lost water to reform the original compound (Supporting Information, Figure S6), as shown by both PXRD and *single crystal X-ray analysis*. In a third experiment, crystals were heated in a Schlenk tube under vacuum to 150 °C for an hour, cooled under dry nitrogen and mounted quickly in the nitrogen stream of the single crystal diffractometer. Single crystal X-ray structural analysis shows that the crystals of **3** have undergone a single-crystal to single-crystal transformation and form compound **3*** at high temperature. Exposure of these dehydrated crystals to moist air for two day results in the reformation of **3**. This single-crystal to single-crystal transformation experiment was repeated a second time on the same two crystals, and again single crystal X-ray analysis at each stage showed the crystals still diffracted, but showed some signs of decay. It is important to note that in these experiments the single crystals are cooled from ambient temperature to 100 K at each step to collect the X-ray data, again indicating the stability of these crystals. In a separate experiment, single crystals were heated in a Schlenk tube under nitrogen to 200 °C for an hour, cooled under nitrogen and mounted quickly in the nitrogen stream of the single crystal diffractometer and again X-ray structural analysis shows that the crystals of **3** had undergone a single-crystal to single-crystal transformation to form compound **3***. TGA experiments show that compound **3*** is stable until 335 °C, well above the decomposition point of the ligand.

As shown in Figure 4b for **4**, decomposition temperatures for compounds **4**–**6** are 280, 227, and 314 °C, respectively. Compounds **4** and **6** maintain single crystallinity upon heating up until 250 and 215 °C, respectively; single crystals heated to these temperatures *still diffract*. Compound **5** does not retain single crystallinity when heated.

Spectral Analyses. Compounds **1**–**6** all display similar fluorescence spectra. Complexes with the $\mathbf{L}_{ala}^-$ ligand all exhibit red-shifted emission spectra when compared to the protonated form, $\mathbf{HL}_{ala}$, and complexes with the $\mathbf{L}_{ser}^-$ ligand all exhibit blue-shifted emission spectra when compared to the protonated form, $\mathbf{HL}_{ser}$. No trends were found between structure type, cation choice, and fluorescence maxima. Fluorescence excitation and emission maxima are given in Table 4.

Table 4. Fluorescence Excitation and Emission Maxima for the Protonated Ligands and Their Compounds

	compound	excitation max (nm)	emission max (nm)
	$\mathbf{HL}_{ala}$	381	450
1	$K(\mathbf{L}_{ala})(MeOH)$	379	469
2	$K(\mathbf{L}_{ala})(H_2O)$	380	462
3	$Na(\mathbf{L}_{ala})(H_2O)$	373	453
6	$Cs(\mathbf{L}_{ala})$	395	465
	$\mathbf{HL}_{ser}$	380	470
4	$K(\mathbf{L}_{ser})$	395	438
5	$Cs(\mathbf{L}_{ser})$	412	427

Second Harmonic Generation. Compounds **1**–**3** and **4**–**6** all contain the naphthalimide chomophore and crystallize in the noncentrosymmetric space groups $P2_12_12_1$ and $P2_1$, respectively, space groups that can potentially generate interesting nonlinear optical behavior. We did not detect any SHG with an incident wavelength of 1064 nm from **1**–**3**. It is possible that these materials do show nonlinear optical SHG activity but at different incident wavelengths. For **4**, **5**, and **6**, powder SHG measurements indicate a SHG efficiency of

dx.doi.org/10.1021/ic401327h | *Inorg. Chem.* 2013, 52, 10041–10051

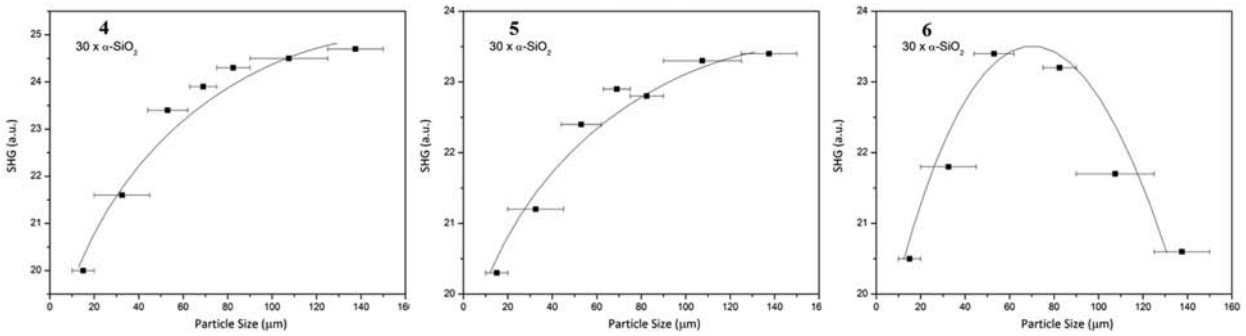

Figure 19. SHG efficiency for compounds **4**−**6** exhibiting type I phase- and nonphase-matching responses.

approximately 30 × α-SiO_2 in the 45−63 μm particle size range. Additional SHG measurements, particle size vs SHG efficiency, indicate that **4** and **5** exhibit type 1 phase-matching while **6** reveals type 1 nonphase-matching behavior. As such **4**−**5** and **6** fall into the class B and C categories, respectively, of SHG materials, as defined by Kurtz and Perry (Figure 19).[14] On the basis of these measurements, we estimate the average NLO susceptibilities, $\langle d_{eff}\rangle_{exp}$, of **4**, **5**, and **6** to be approximately 6.3, 6.3, and 3.0 pm/V, respectively.

DISCUSSION

Eight new complexes of three different alkali metals (Na^+, K^+, and Cs^+) have been prepared from the two ligands pictured in Scheme 1, ligands that contain a carboxylate donor group, an enantiopure chiral center, and a 1,8-naphthalimide $\pi\cdots\pi$ stacking supramolecular tecton. Even though there is a large change in ionic radii with these three metals (six-coordinate ionic radii of 1.02, 1.46, and 1.67 Å for Na^+, K^+, and Cs^+, respectively[17]), each of the new complexes has a solid state structure based on six-coordinate metals linked into homochiral helical rod SBU central cores, with the exception of compounds **2*** and **3*** which have lost solvent upon heating and contain 5-coordinate potassium or sodium cations, respectively. Despite this uniformity of structure, the helical rod SBU cores form from four different, but related bonding arrangements: in **1**, **4**, and **5** the metal polyhedra are linked by edge-sharing through bridging oxygens originating from the alcohol and carboxylate; in **2**, **2***, and **3*** by corner-sharing through bridging oxygens originating from the carboxylate; in **3** by corner-sharing through bridging oxygens originating from the water; and in **6** by edge-sharing through bridging oxygens originating only from the carboxylate. Very few homochiral helical rod SBUs have been reported previously.[19] Also, this consistent formation of a central organizational structural feature in the work described here is uncommon for group 1 carboxylates.[12]

In addition to this consistent formation of a similar type of SBU, only two overall structural arrangements of the eight complexes are observed. The five complexes **1**−**3*** are all three-dimensional rod-packed structures in a uninodal 4*c* net, in which the remaining two dimensions are linked by the interactions of oxygens on the naphthalimide groups bridging to adjacent SBUs forming a "square" arrangement. In contrast, complexes **4**−**6** show polar covalent linkages in only one additional dimension leading to the formation of two-dimensional sheets. This inter-rod bonding to the group 1 metal of the carbonyl oxygens coupled with intrarod bonding of the same type present in all eight complexes is a new bonding feature of ligands containing the naphthalimide group that was not present in our previous work with transition metal complexes. Such a difference is not unexpected in complexes of these oxophilic metals.

In all of our previous chemistry with these types of naphthalimide-based ligands, we have observed structures strongly influenced by strong $\pi\cdots\pi$ stacking interactions. In addition to complexes **1**−**3*** having three-dimensional "covalent" structures, they are also supported by these supramolecular interactions. More importantly, in the structures of complexes **4**−**6**, the third dimension is supported exclusively by interdigitated $\pi\cdots\pi$ stacking interactions, forming SMOF solids. As can be seen in Figure 13, Supporting Information, Figures S4 and S5, the overlap of the naphthalimide rings in complexes **4**−**6** is somewhat reduced when compared to that in complexes **1**−**3***, a result emphasized by the "slippage" parameters in Tables 2 and 3, but the overlap is still substantial. It is interesting to speculate that these noncovalent forces are instrumental not only in the organization of the third dimension in complexes **4**−**6**, but also in the consistency of the structures based on homochiral helical SBUs in all eight complexes reported here. This impact of the naphthalimide supramolecular tecton is supported by the fact that all of the metals have low coordination numbers, most notably the five-coordinate potassium cation in **2***, the five-coordinate sodium cation in **3*** and the six-coordinate cesium cations in compounds **5** and **6**, all particularly low for these large cations.[20]

A related interesting result of this chemistry is the limited amount of coordinated solvent in all the structures. In general, group 1 complexes crystallized from polar solvents, especially those of the heavier metals, retain a significant amount of solvent,[12] and this issue has been shown to impact on the dimensionality and thermal stability of the structures.[12] Complexes **1**−**3** contain only one equivalent of solvent in the structures. Heating complexes **2** and **3** formed new complexes, **2*** and **3***, respectively, which have no solvent. Complexes **4** and **5** contain no solvent by design; after obtaining the result of one methanol in the structure of **1** we synthesized the $\mathbf{L_{ser}}^-$ ligand that "builds in" the alcohol functional group to intentionally prepare complexes that contained no solvent. While this *designed ligand modification* is successful in the initial goal of eliminating the solvent, the resulting tridentate bonding of the new ligand also caused a structural change from three- to two-dimensional as described above. The absence of solvent in complex **6** is especially notable as the large cesium cation is only six-coordinate and has a "vacant face" in its structure. We note that although the coordination sphere of **6** has this highly distorted arrangement of the ligands, there are apparently at least two Cs−H interactions (Figure 16 b). Again, as indicated above, it is likely that the large naphthalimide groups coupled

dx.doi.org/10.1021/ic401327h | *Inorg. Chem.* 2013, 52, 10041−10051

with the $\pi\cdots\pi$ stacking interactions strongly influence the amount of solvent and relatively low coordination numbers in these structures.

The presence of solvent makes a substantial impact on the thermal properties. Compound **1** loses the bridging methanol upon heating resulting in a polycrystalline powder (**1p**) which is stable up to the decomposition point around 318 °C. Although this loss of solvent results in collapse of the single crystal structure, this desolvated solid can be recrystallized to reform the starting structure. In the cases of compounds **2** and **3**, coordinated water can be reversibly removed/incorporated into the structure by heating in the absence of water vapor and cooling in the presence of water vapor through *gas/solid, single-crystal to single-crystal transformations*. In the case of compound **2** there is no huge impact on the crystal structure from the transformation, likely a function of the fact that the water molecule is a terminal ligand. The loss of water results in a 5-coordinate potassium cation, which is unusually low, and a slight decrease of the unit cell volume. Upon heating compound **3**, the water that is *the only bridge* between the sodium cations was lost, but the crystals *remain suitable for single crystal X-ray analysis*. In the structure of this new compound, **3***, the role of the carboxylate group changed from κ^2 to μ^2-κ^1:κ^2 and O3 rotates 1.36 Å closer to the adjacent sodium cation to form a direct interaction to satisfy the coordination environment of the sodium cations and retain the homochiral helical rod SBU structure (Figure 20). Exposure of

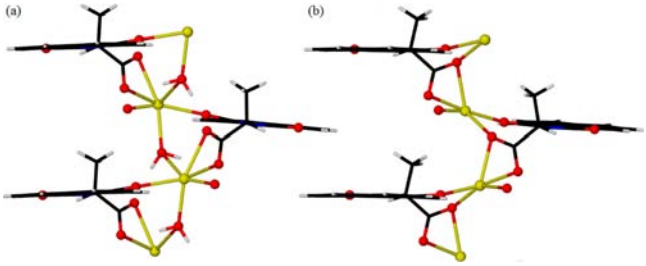

Figure 20. Comparison of hydrated **3** (a) and dehydrated **3*** (b) and the differences in carboxylate bonding; black, C; red, O; blue, N; white, H; yellow, Na.

the single crystals of **3*** to moist air over the course of three days results in a reincorporation of water into the bridging position of the rods reforming **3**, again *without loss of single crystallinity*. This reversible single-crystal to single-crystal transformation can be repeated a second time, but with modest degradation of the crystal (note the crystals are cooled to 100 K at each step for the analysis). It can be argued that this structural change is supported by the intrarod chelate rings formed by the carboxylate and naphthalimide carbonyl, which change from a nine-member ring in **3** to a seven member ring in **3***. Remarkably, these reversible single-crystal to single-crystal transformations occur in the absence of channels. In contrast to the solvated crystals, crystals of solvent free compounds **4** and **6** are amazingly stable; they retain single crystallinity up to about 210 °C, well above the decomposition point of the protonated ligand. This stability is particularly notable for an SMOF solid, where at least one dimension is organized only by noncovalent forces.

All of the compounds exhibit luminescence which is known to be derived from the naphthalimide ligand. Compounds containing the L_{ala}^- ligand (**1**–**3**, **6**) are all red-shifted by 3–19 nm with respect to crystals of the protonated ligand whereas compounds containing the L_{ser}^- ligand (**4**, **5**) are both blue-shifted by 32–43 nm with respect to the crystals of the protonated ligand.

The SHG efficiency of these compounds was studied for several reasons: the naphthalimide ring is a known chromophore, the ligands are enantiopure and lead to the formation of crystals with noncentrosymmetric space groups, and rod shaped SBUs are known to promote interesting electronic properties because of the extended metal–metal interactions.[21] Compounds **1**–**3** did not exhibit observable SHG efficiency at an incident wavelength of 1064 nm, but compounds **4**–**6** did exhibit modest SHG efficiency for MOF-like compounds in the range of 30 × α-SiO_2. Compounds **4** and **5** exhibit type I phase-matching behavior while compound **6** is type I nonphase matchable. The SHG effect in **4**–**6** is thought to originate from the lower symmetry of these networks because **1**–**6** contain the same building blocks: enantiopure helical rods of alkali metals and $\pi\cdots\pi$ stacking. The strong SHG response coupled with the retention of crystallinity at elevated temperatures makes compounds **4**–**6** potential candidates for practical applications.

■ ASSOCIATED CONTENT

Supporting Information

X-ray crystallographic files in CIF format for the structural determinations, artwork depicting the 3D architectures and naphthalimide overlap for compounds **2** (Figure S1), **3** (Figure S2), **3*** (Figure S3), **5** (Figure S4), and **6** (Figure S5), TGA experiment on compound **3** (Figure S6), PXRD data for **1p** (Figure S7) and PXRD data showing the phase purity of compounds **1**–**6** (Figures S8–S13). This material is available free of charge via the Internet at http://pubs.acs.org.

■ AUTHOR INFORMATION

Corresponding Author

*E-mail: reger@mailbox.sc.edu.

Notes

The authors declare no competing financial interest.

■ ACKNOWLEDGMENTS

The authors acknowledge with thanks the financial support of the National Science Foundation through Grant CHE-1011736. We thank Cory Read for running the powder XRD. P.S.H. and T.T.T. thank the Welch Foundation (Grant E-1457) for support.

■ REFERENCES

(1) (a) Corma, A.; Garcia, H.; Llabrés i Xamena, F. X. *Chem. Rev.* **2010**, *110*, 4606. (b) Lin, W. *Top. Catal.* **2010**, *53*, 869. (c) Natori, Y.; Tsutsui, H.; Sato, N.; Nakamura, H.; Nambu, H.; Shiro, M.; Hashimoto, S. *J. Org. Chem.* **2009**, *74*, 4418.

(2) (a) Tranchemontagne, D. J.; Mendoza-Cortés, J. L.; O'Keefe, M.; Yachi, O. M. *Chem. Soc. Rev.* **2009**, *38*, 1257–1283. (b) Rosi, N. L.; Kim, J.; Eddaoudi, M.; Chem, B.; O'Keeffe, M.; Yaghi, O. M. *J. Am. Chem. Soc.* **2005**, *127*, 1504–1518. (c) O'Keeffe, M.; Yaghi, O. M. *Chem. Rev.* **2012**, *112*, 675–702.

(3) (a) Design of Organic Solids. Weber, E., Ed.; *Topics in Current Chemistry*; Springer: Berlin, Germany, 1998; Vol. *198*. (b) Pidcock, E.; Motherwell, W. D. S. *Cryst. Growth Des.* **2005**, *5*, 2232. (c) Du, M.; Zhang, Z. H.; Zhao, X. J. *Cryst. Growth Des.* **2005**, *5*, 1199. (d) Takahashi, S.; Katagiri, T.; Uneyama, K. *Chem. Commun.* **2005**, 3658. (e) Weatherhead-Kloster, R. A.; Selby, H. D.; Miller, W. B.; Mash, E. A. *J. Org. Chem.* **2005**, *70*, 8693. (f) Zhang, J. P.; Lin, Y.-Y.;

Huang, X. C.; Chen, X.-M. *Chem. Commun.* **2005**, 1258. (g) Vangala, V. R.; Bhogala, B. R.; Dey, A.; Desiraju, G. R.; Broder, C. K.; Smith, P. S.; Mondal, R.; Howard, J. A. K.; Wilson, C. C. *J. Am. Chem. Soc.* **2003**, *125*, 14495.
(4) (a) Reger, D. L.; Horger, J. J.; Smith, M. D.; Long, G. J.; Grandjean, F. *Inorg. Chem.* **2011**, *50*, 686−704. (b) Reger, D. L.; Horger, J. J.; Smith, M. D. *Chem. Commun.* **2011**, *47*, 2805−2807. (c) Reger, D. L.; Horger, J. J.; Debreczeni, A.; Smith, M. D. *Inorg. Chem.* **2011**, *50*, 10225−10240.
(5) (a) Qu, Z.-R.; Zhao, H.; Wang, X.-S.; Li, Y.-H.; Song, Y.-M.; Liu, Y.-J.; Ye, Q.; Xiong, R.-G.; Abrahams, B. F.; Xue, Z.-L.; You, X.-Z. *Inorg. Chem.* **2003**, *42*, 7710−7712. (b) Ingleson, M. J.; Bacsa, J.; Rosseinsky, M. J. *Chem. Commun.* **2007**, *29*, 3036−3038.
(6) (a) Rombach, M.; Gelinsky, M.; Vahrenkamp, H. *Inorg. Chim. Acta* **2002**, *334*, 25−33. (b) Fox, S.; Buesching, I.; Barklage, W.; Strasdeit, H. *Inorg. Chem.* **2007**, *46*, 818−824.
(7) (a) Reger, D. L.; Debreczeni, A.; Smith, M. D. *Inorg. Chem.* **2011**, *50*, 11754−11764. (b) Reger, D. L.; Debreczeni, A.; Smith, M. D..; Jezierska, J.; Ozarowski, A. *Inorg. Chem.* **2012**, *51*, 1068−1083. (c) Reger, D. L.; Debreczeni, A.; Reinecke, B.; Rassolov, V.; Smith, M. D.; Semeniuc, R. F. *Inorg. Chem.* **2009**, *48*, 8911−8924.
(8) Reger, D. L.; Debreczeni, A.; Horger, J. J.; Smith, M. D. *Cryst. Growth Des.* **2011**, *11*, 4068−4079.
(9) Lee, J. D. *Concise Inorganic Chemistry*; Chapman & Hall: New York, 1991.
(10) (a) Takarada, T.; Nabatame, T.; Ohtsuka, Y.; Tomita, A. *Ind. Eng. Chem. Res.* **1989**, *28*, 505−510. (b) Makosza, M.; Nieczypor, P.; Grela, K. *Tetrahedron* **1998**, *54*, 10827−10836.
(11) (a) Valasek, J. *Phys. Rev.* **1921**, *17*, 475. (b) Kambay, S.; Brezina, B.; Petzelt, J.; Schaack, G. *J. Phys.: Condens. Matter* **1996**, *8*, 8669.
(12) (a) Fromm, K. M. *Coord. Chem. Rev.* **2008**, *252*, 856−885. (b) Banerjee, D.; Parise, J. B. *Cryst. Growth Des.* **2011**, *11*, 4704−472.
(13) Reger, D. L.; Leitner, A. P.; Smith, M. D. *Inorg. Chem.* **2012**, *51*, 10071−10073.
(14) Kurtz, S. K.; Perry, T. T. *J. Appl. Phys.* **1968**, *39*, 3798.
(15) Ok, K. M.; Chi, E. O.; Halasyamani, P. S. *Chem. Soc. Rev.* **2006**, *35*, 710.
(16) *SMART Version 5.630, SAINT+ Version 6.45 and SADABS Version 2.10*; Bruker Analytical X-ray Systems, Inc.: Madison, WI, 2003.
(17) Sheldrick, G. M. *Acta Crystallogr.* **2008**, *A64*, 112.
(18) Dolomanov, O. V.; Bourhis, L. J.; Gildea, R. J.; Howard, J. A. K.; Puschmann, H. *J. Appl. Crystallogr.* **2009**, *42*, 339.
(19) (a) Mallick, A.; Saha, S.; Pachfule, P.; Roy, S.; Banerjee, R. *J. Mater. Chem.* **2010**, *20*, 9073. (b) Appelhans, L. N.; Kosa, M.; Radha, A. V.; Simoncic, P.; Navrotsky, A.; Parrinello, M.; Cheetham, A. K. *J. Am. Chem. Soc.* **2009**, *131*, 15375. (c) Yeung, H. H.-M.; Kosa, M.; Parrinello, M.; Forster, P. M.; Cheetham, A. K. *Cryst. Growth Des.* **2011**, *11*, 221. (d) Rood, J. A.; Noll, B. C.; Henderson, K. W. *J. Solid State Chem.* **2010**, *183*, 270. (e) Gao, Q.; Wang, X.; Conato, M. T.; Makerenko, T.; Jacobson, A. J. *Cryst. Growth Des.* **2011**, *11*, 4632.
(20) (a) Nichol, G. S.; Clegg, W. *Polyhedron* **2006**, *25*, 1043−1056. (b) Stein, I.; Ruschewitz, U. *Acta Crystallogr., Sect. E* **2007**, *63*, M382−M84. (c) Wiesbrock, F.; Schmidbaur, H. *Inorg. Chem.* **2003**, *42*, 7283−7289. (d) Santra, S.; Das, B.; Baruah, J. *J. Chem. Crystallogr.* **2011**, *41*, 1981−1987.
(21) (a) Xu, X.; Zhang, X.; Liu, X.; Sun, T.; Wang, E. *Cryst. Growth Des.* **2010**, *10*, 2272−2277. (b) Che, C.-M.; Tse, M.-C.; Chan, M. C. W.; Cheung, K.-K.; Phillips, D. L.; Leung, K.-H. *J. Am. Chem. Soc.* **2000**, *122*, 2464−2468.